Universal rescaling of drop impact on smooth and rough surfaces

J. Fluid Mech. (2016), *vol.* 786, R4, doi:10.1017/jfm.2015.620

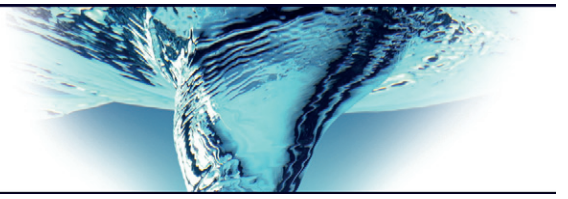

JFM RAPIDS
journals.cambridge.org/rapids

Universal rescaling of drop impact on smooth and rough surfaces

J. B. Lee[1], N. Laan[2], K. G. de Bruin[3], G. Skantzaris[2], N. Shahidzadeh[2], D. Derome[4], J. Carmeliet[1,4,†] and D. Bonn[2]

[1]Chair of Building Physics, ETH Zürich, Stefano-Franscini-Platz 5, CH-8093 Zürich, Switzerland

[2]Van der Waals-Zeeman Institute, Institute of Physics, University of Amsterdam, Science Park 904, 1098 XH Amsterdam, Netherlands

[3]Netherlands Forensic Institute, Laan van Ypenburg 6, 2497 GB The Hague, Netherlands

[4]Laboratory for Multiscale Studies in Building Physics, Swiss Federal Laboratories for Materials Science and Technology, EMPA, Überlandstrasse 129, CH-8600 Dübendorf, Switzerland

(Received 19 August 2015; revised 19 August 2015; accepted 20 October 2015; first published online 30 November 2015)

The maximum spreading of drops impacting on smooth and rough surfaces is measured from low to high impact velocity for liquids with different surface tensions and viscosities. We demonstrate that dynamic wetting plays an important role in the spreading at low velocity, characterized by the dynamic contact angle at maximum spreading. In the energy balance, we account for the dynamic wettability by introducing the capillary energy at zero impact velocity, which relates to the spreading ratio at zero impact velocity. Correcting the measured spreading ratio by the spreading ratio at zero velocity, we find a correct scaling behaviour for low and high impact velocity and, by interpolation between the two, we find a universal scaling curve. The influence of the liquid as well as the nature and roughness of the surface are taken into account properly by rescaling with the spreading ratio at zero velocity, which, as demonstrated, is equivalent to accounting for the dynamic contact angle.

Key words: contact line, drops, interfacial flows (free surface)

1. Introduction

The maximal spreading of a liquid drop impact on a solid surface is relevant for many applications in natural, agricultural and industrial processes, such as raindrop impact (Abuku *et al.* 2009; Joung & Buie 2015; Zhao *et al.* 2015), pesticide deposition (Wirth, Storp & Jacobsen 1991; Bergeron *et al.* 2000), thermal spraying (McDonald *et al.* 2006), inkjet printing (Derby 2010) and even within bloodstain

†Email address for correspondence: carmeliet@arch.ethz.ch

pattern analysis, where one requires the velocity of a blood drop for crime scene reconstruction (Laan *et al.* 2015). An understanding of the maximum spreading of drop impact is key to controlling the drop dynamics in these applications (Rioboo, Tropea & Marengo 2001; Yarin 2006). For example, in the case of raindrop impact on soil or a building, the wetted area for liquid transport into the substrate is directly related to the maximum spreading (Erkal, D'Ayala & Sequeira 2012; Blocken & Carmeliet 2015).

Drop impact and its maximal spreading are governed by a balance between kinetic energy, capillary energy and viscous dissipation during spreading. The models are commonly formulated using two dimensionless parameters: the Weber number ($We \equiv \rho D_0 V_i^2/\gamma$), describing the ratio between the kinetic and capillary energy, and the Reynolds number ($Re \equiv \rho D_0 V_i/\mu$), describing the ratio between the kinetic and viscous energy. Here, D_0 is the initial droplet diameter, V_i is the impact velocity, ρ is the liquid density, γ is the surface tension and μ is the viscosity.

Different models have been proposed for the maximum spreading ratio $\beta_{max} = D_{max}/D_0$ (Roisman, Rioboo & Tropea 2002), where D_{max} is the maximum spreading diameter. Studies distinguish two main domains: the capillary regime at low impact velocity and the viscous regime at high impact velocity (Clanet *et al.* 2004). For the viscous regime, based on energy conservation between kinetic and viscous dissipation energy, a scaling of β_{max} with $Re^{1/5}$ is found (Madejski 1976; Roisman *et al.* 2002). Based on an energy approach for a pancake-shaped droplet at maximum spreading, including kinetic and surface energy before impact and surface energy and viscous dissipation at maximum spreading, a scaling with $Re^{1/4}$ is found (Pasandideh-Fard *et al.* 1996). Clanet *et al.* (2004) proposed, based on momentum conservation, a scaling of β_{max} with $We^{1/4}$. Laan *et al.* (2014) showed that, even though the scaling with $We^{1/4}$ seems consistent for some liquids, such as water, it is not for other liquids, like blood. Based on energy conservation between kinetic and surface energy, a scaling of β_{max} with $We^{1/2}$ is found (Collings *et al.* 1990; Bechtel, Bogy & Talke 1993). However, Laan *et al.* (2014) showed that none of their data scaled with the dependences reported in the literature ($Re^{1/4}$, $Re^{1/5}$, $We^{1/4}$ and $We^{1/2}$). Therefore, they proposed a solution that introduces a broad cross-over regime between the low and high impact velocities by interpolating between $We^{1/2}$ and $Re^{1/5}$. The interpolation between the two scaling laws showed good agreement with experimental data. This method thus demonstrated clearly that droplet spreading cannot be predicted simply by equating the kinetic energy either to the capillary energy or to the viscous dissipation, since in most cases of practical interest, all three energies are important. However, Laan's approach implies that at zero impact velocity the spreading ratio equals zero, which is physically impossible. This means that the liquid wettability on the surface will play a role, determining the spreading ratio at low impact velocity.

In this study, we examine how the wettability of a liquid on a surface influences the maximum spreading at low impact velocity. Therefore, we performed droplet impact experiments with various liquids on smooth surfaces with varying wettability. In addition, we repeated the experiments on rough surfaces, where we show that no additional parameters are required for these kinds of surfaces. More specifically, the aim of this study is to extend the approach of Laan *et al.* (2014) in order to include the dynamic wettability.

2. Drop impact experiments

To analyse the influence of the surface tension and viscosity of liquid, five liquids are used: pure ethanol (ethanol), deionized water (water), 1:1 glycerol–water

	Liquid properties			Impact condition			
	ρ (kg m^{-3})	μ (Pa s)	γ (N m^{-1})	D_0 (mm)	V_i (m s^{-1})	We	Re
Ethanol	789	1.2×10^{-3}	2.3×10^{-2}	1.8	0.2–2.7	2–500	250–3500
Water	998	1.0×10^{-3}	7.3×10^{-2}	1.8–3.6	0.2–5.0	1–1300	450–18 000
Glycerol 6 mPa s	1124	6.0×10^{-3}	6.6×10^{-2}	2.0–3.3	0.2–5.0	1–1500	60–3200
Glycerol 10 mPa s	1158	1.0×10^{-2}	6.8×10^{-2}	1.8	0.2–3.7	1–430	40–800
Glycerol 51 mPa s	1204	5.1×10^{-2}	6.5×10^{-2}	2.0–3.2	1.0–5.0	35–1500	45–400

TABLE 1. Physical properties of liquids and droplet impact conditions.

	Smooth surface			Rough surface					
Parameter	Glass	Steel	Parafilm	P120	P240	P600	P2500	GB	SB
R_a (μm)	0.2	0.4	0.5	20.8	12.1	6.2	2.7	9.5	4.7
Averaged particle dia. (μm)	—	—	—	125.0	58.5	25.8	8.4	30.0–50.0	—

TABLE 2. Roughness and particle size of surfaces.

	Glass		Steel		Parafilm	
	θ_{eq} (deg.)	θ_D (deg.)	θ_{eq} (deg.)	θ_D (deg.)	θ_{eq} (deg.)	θ_D (deg.)
Ethanol	∼0	52	∼0	44	21	63
Water	23	94	61	103	110	108
Glycerol 10 mPa s	22	123	52	121	94	116

TABLE 3. Equilibrium and dynamic contact angles for different surfaces and liquids.

mixture (glycerol 6 mPa s), 1:1.3 glycerol–water mixture (glycerol 10 mPa s) and 1:3 glycerol–water mixture (glycerol 51 mPa s). The liquid density ρ, viscosity μ and surface tension γ are reported in table 1.

We selected three smooth surfaces with an arithmetic average roughness $R_a < 0.5$ μm: glass, steel and parafilm. The parafilm substrate is prepared on slide glass with a plastic paraffin film (PARAFILM M, Sigma-Aldrich). The rough surfaces are sandpaper (Silicon Carbide Paper, Buehler) with different grit sizes (P120, P240, P600 and P2500), a monolayer of glass beads sintered to a glass surface (GB) and a sandblasted glass slide (SB). The roughness is measured by a contact profilometer (Surftest-211, Mitutoyo) equipped with a 5 μm radius diamond-tipped stylus. The roughness R_a for the different surfaces is given in table 2.

The wettability in equilibrium conditions is characterized by the contact angle of the droplet. The contact angle θ_{eq} is determined with a 3 μl sessile droplet in equilibrium (no movement) after gentle deposition from a needle. The equilibrium contact angle is obtained from a polynomial fit to the outline of the liquid–vapour interface (table 3). At equilibrium conditions, glass and steel are wetting surfaces for all liquids, while parafilm is wetting for ethanol and non-wetting for water and glycerol.

Droplets are generated at a flat-tipped needle by means of the pendant method. The syringe pump pushes the liquid at the rate of 20 μl min^{-1} though the needle until a single droplet detaches. The drop impact is recorded in shadowgraphy using a high-speed camera (10 000 f.p.s., 7.38 μm spatial resolution and 5 μs exposure time). The impact velocity is varied by varying the height of the needle above the surface. The impact velocity is increased until splashing (prompt splash) starts to

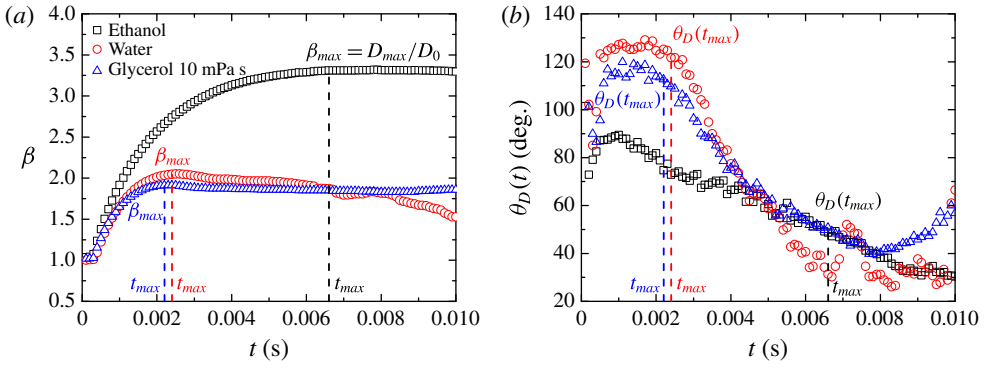

FIGURE 1. Time evolution of (*a*) the spreading ratio and (*b*) the dynamic contact angle for different liquids. The vertical lines indicate the time at maximal spreading.

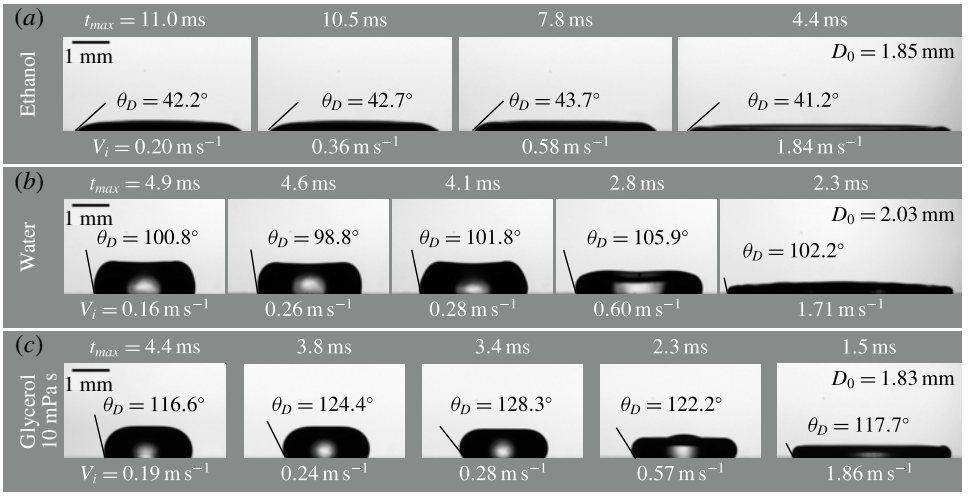

FIGURE 2. Snapshots of droplets impacting on a steel surface at maximal spreading as a function of impact velocity ($V_i = 0.2$–1.8 m s^{-1}): (*a*) ethanol, (*b*) water, (*c*) glycerol 10 mPa s.

occur. The impact conditions are given in table 1. Droplet impact for each measuring condition is repeated at least three times. A custom-made image analysis MATLAB code is used to measure the initial droplet diameter D_0, the impact velocity V_i, the spreading diameter $D(t)$, the dynamic contact angle $\theta_D(t)$, the maximum spreading diameter D_{max} at t_{max} and the dynamic contact angle at maximum spreading $\theta_D(t_{max})$. The dynamic contact angle is obtained from the image by applying a goniometric mask (Biolè & Bertola 2015) on the region of 100 μm vertically above the surface line. As an example, figure 1 shows the typical time evolution of the spreading ratio $\beta(t) = D(t)/D_0$, the dynamic contact angle $\theta_D(t)$, as well as the maximum spreading ratio β_{max} and the dynamic contact angle at maximum spreading $\theta_D(t_{max})$ for three liquids on a steel surface with $V_i \sim 1.0$ m s^{-1}.

Figure 2 shows snapshots of ethanol, water and glycerol 10 mPa s impacting on a smooth steel surface at maximum spreading for different impact velocities ($V_i =$ 0.2–1.8 m s^{-1}). The maximum spreading ratio β_{max} increases with impact velocity

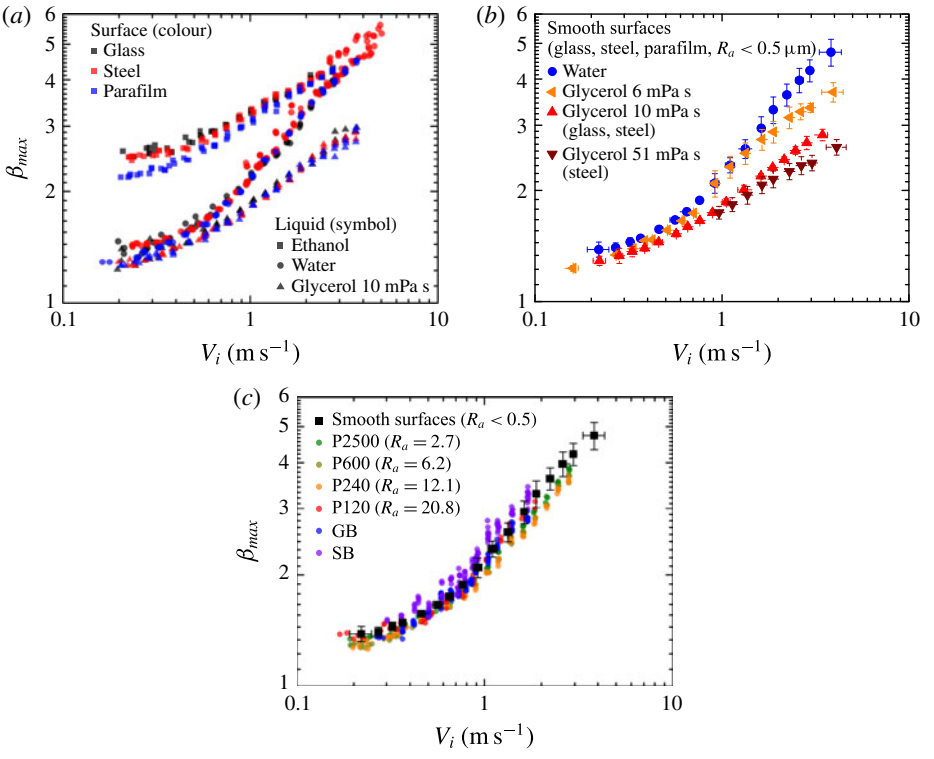

FIGURE 3. Maximum spreading ratio versus impact velocity. (*a*) Different liquids on different smooth surfaces. (*b*) Influence of viscosity (smooth surfaces). (*c*) Influence of roughness (liquid = water).

for all three liquids. Ethanol spreads further and reaches its maximum spreading later in time than water and glycerol. The dynamic contact angle at maximum spreading, also indicated in the figure, is approximately constant over the impact velocity range. We report the average values of the dynamic contact angle at maximum spreading in table 3. The dynamic contact angle of ethanol lies in the range of 44°–63°, which is higher than the equilibrium contact angle (21°). Water and glycerol also show a higher dynamic contact angle (94°–123°) than the equilibrium contact angle (22°–61°) for glass and steel, while for parafilm the equilibrium and dynamic contact angles are equal (approximately 110°). For completeness, the time at maximum spreading, t_{max}, is indicated in the images, which decreases with impact velocity.

There is a clear distinction in the maximum spreading ratio β_{max} between the different liquids on the smooth surfaces (glass, steel and parafilm) as a function of the impact velocity (figure 3*a*). Given a specific liquid, the maximum spreading ratio is almost identical for all of the smooth surfaces. Accordingly, we argue that the liquid, not the substrate, plays the most important role. Ethanol shows the highest maximum spreading, while glycerol shows the lowest maximum spreading. The maximum spreading of water shows a transition between the glycerol at low impact velocity and the ethanol at high impact velocity. At low impact velocity, the spreading is similar for water and glycerol as their values of surface tension are similar. We may conclude that the nature of the substrate has only a small influence on the

spreading and, with a proper rescaling by the surface wettability, we will show that this influence disappears (see below).

Figure 3(*b*) shows the maximum spreading ratio for liquids of increasing viscosity: water and water–glycerol mixtures 6, 10 and 51 mPa s respectively. The liquid viscosity limits the spreading at high velocity, but does not influence the spreading at low velocity, where all curves tend to acquire similar values.

Figure 3(*c*) shows the maximum spreading ratio for water on rough surfaces: four sandpapers of different roughnesses, monolayered sintered glass beads (GB) and sandblasted glass (SB). Although the surfaces have different roughness and equilibrium wetting characteristics, the maximum spreading ratio is almost identical for all of them and is equal to the spreading ratio on a smooth surface. We therefore conclude that the roughness of the substrate has a rather small influence on the spreading. We will further show that, when we rescale the curves for different liquids and substrates taking into account the dynamic wetting behaviour at low velocity, all curves collapse onto a single curve.

3. Scaling of the maximum spreading diameter

When considering the energy balance of a droplet impacting on a solid substrate, the kinetic energy, the capillary energy and the viscous dissipation have to be taken into account. During impact, the spreading droplet deforms until it reaches its maximum diameter D_{max} within a few milliseconds. The capillary energy can then be written as $E_\gamma \sim \gamma D_{max}^2$ and the energy dissipated by viscous forces as $E_\mu \sim \mu V_i D_{max}^5 / D_0^3$ (Madejski 1976; Collings *et al.* 1990). In the capillary limit, we can assume that kinetic energy is transformed into capillary energy, $E_k \sim E_\gamma$. In this regime, the maximum spreading ratio scales as $\beta_{max} \sim We^{1/2}$ (Bechtel *et al.* 1993; Eggers *et al.* 2010). In the viscous limit, the kinetic energy is totally transformed into viscous energy, $E_k \sim E_\mu$. Then, the maximum spreading ratio scales as $\beta_{max} \sim Re^{1/5}$ (Madejski 1976; Chandra & Avedisian 1991). The scaling of $\beta_{max} \sim We^{1/2}$ implies that, at zero impact velocity, the spreading ratio equals zero, which is physically impossible ($\beta_{max} \geqslant 1$). At low impact velocity, the spreading ratio does not tend to zero, but levels off to a limiting value, which is referred to in the following as $\beta_{V_i \to 0}$ (figure 4).

The spreading ratio $\beta_{V_i \to 0}$ is determined by approximating the measured data by the function

$$\beta_{max} = \beta_{Vi \to 0} + A \frac{V_i^C}{B + V_i^C}, \tag{3.1}$$

where A, B, C and $\beta_{V_i \to 0}$ are fitting parameters. Figure 4 shows that (3.1) describes the measured data for liquid droplets on a steel surface satisfactorily. Table 4 gives the values for $\beta_{V_i \to 0}$ on different substrates and for different liquids.

When we assume that the spreading droplet attains the form of a spherical cap while it keeps a constant volume (Berthier & Beebe 2007), the spreading ratio $\beta_{V_i \to 0}$ can be related to a contact angle $\theta_{V_i \to 0}$. It is necessary to discern between the cases for a hydrophilic surface ($\theta_{V_i \to 0} < 90°$) and a hydrophobic surface ($\theta_{V_i \to 0} > 90°$). The spreading ratio is given by

$$\beta_{V_i \to 0} = \begin{cases} \left(\dfrac{4 \sin^3 \theta_{V_i \to 0}}{2 - 3 \cos \theta_{V_i \to 0} + \cos^3 \theta_{V_i \to 0}} \right)^{1/3} & \text{if } \theta_{V_i \to 0} < 90°, \\ \left(\dfrac{1}{(2 + \cos \theta_{V_i \to 0}) \sin^4 (\theta_{V_i \to 0}/2)} \right)^{1/3} & \text{if } \theta_{V_i \to 0} > 90°. \end{cases} \tag{3.2}$$

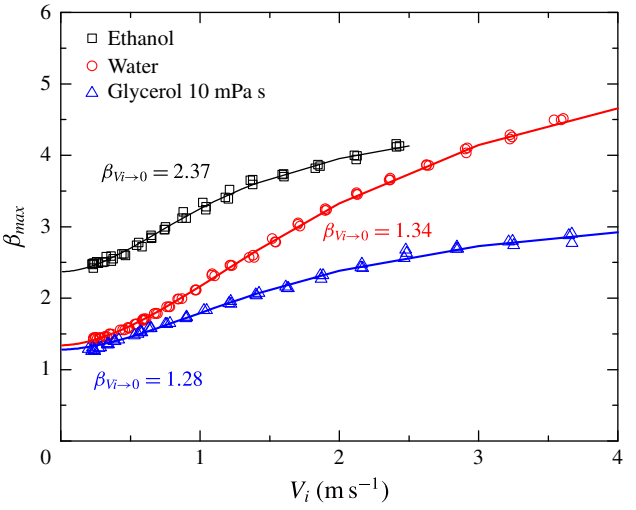

FIGURE 4. Example of the determination of the maximum spreading ratio at zero impact velocity $\beta_{V_i\to 0}$ by fitting (3.1) to the measured data.

	Ethanol	Water	Glycerol (mPa s)		
			6	10	51
Glass	2.45	1.30	—	1.29	—
Steel	2.37	1.34	1.24	1.28	1.24
Parafilm	2.09	1.25	—	1.24	—
P2500	—	1.24	—	—	—
P600	—	1.21	—	—	—
P240	—	1.23	—	—	—
P120	—	1.29	—	—	—
GB	—	1.20	—	—	—
SB	—	1.30	—	—	—

TABLE 4. Spreading ratio $\beta_{Vi\to 0}$ at zero impact velocity.

This equation allows determination of a contact angle $\theta_{V_i\to 0}$ given a value of $\beta_{V_i\to 0}$. Figure 5(*a*) compares the dynamic contact angle $\theta_D(t_{max})$, determined from experiments, and the contact angle $\theta_{V_i\to 0}$, determined from $\beta_{V_i\to 0}$ using (3.2). Regardless of a constant offset, the contact angle $\theta_{V_i\to 0}$ predicts fairly well the measured contact angles during dynamic wetting $\theta_D(t_{max})$. The offset is attributed to an empty volume in the spherical cap model (see figure 5*a*,*b*), since the real droplet shape does not totally resemble a spherical cap but rather acquires the form of a pancake. The missing volume leads to an underprediction of the contact angle by the spherical cap model.

The aim of this analysis is to demonstrate that dynamic wetting plays an important role in the spreading at low velocities, and that the dynamic wetting as characterized by the dynamic contact angle θ_D has to be taken into account in predicting the maximum spreading. The analysis above shows that the capillary energy related to $\theta_{V_i\to 0}$ or to $\beta_{V_i\to 0}$ has to be incorporated in the maximum spreading model.

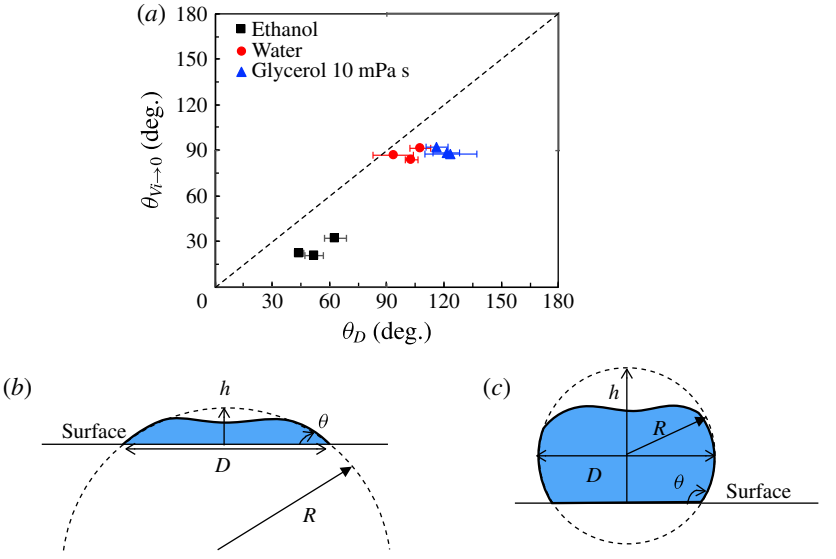

FIGURE 5. (*a*) Comparison of the dynamic contact angle $\theta_D(t_{max})$ (from experiments) and the contact angle $\theta_{V_i\to 0}$ determined from $\beta_{V_i\to 0}$ using (3.2). (*b*,*c*) Spherical cap representation of a droplet with height h, radius R, maximum droplet diameter D and corresponding contact angle θ: (*b*) $\theta < 90°$, (*c*) $\theta > 90°$.

To do so, we add the capillary energy $E_{\gamma 0} \sim \gamma D_{V_i\to 0}^2$ in the low-velocity limit, where $D_{V_i\to 0} = \beta_{V_i\to 0} D_0$. Then, the energy balance reads

$$E_k + E_{\gamma 0} \sim E_\gamma \quad \text{or} \quad \rho D_0^3 V_i^2 + \gamma D_{V_i\to 0}^2 = \gamma D_{max}^2, \tag{3.3a,b}$$

which leads to

$$\sqrt{\beta_{max}^2 - \beta_{V_i\to 0}^2} = We^{1/2}. \tag{3.4}$$

Equation (3.4) shows that we can still assume a scaling with $We^{1/2}$ after a correction for dynamic wetting using the maximum spreading ratio at zero velocity $\beta_{V_i\to 0}$ as from (3.1). After correction, the maximum spreading should still scale with $We^{1/2}$ and $Re^{1/5}$ at low and high velocities respectively. Similarly to Laan *et al.* (2014), the interpolation between the low- and high-impact-velocity regimes can be written as

$$\left(\beta_{max}^2 - \beta_{V_i\to 0}^2\right)^{1/2} \propto Re^{1/5} f(We). \tag{3.5}$$

The function f allows a smooth cross-over between the two limits where only one fitting parameter is required to successfully describe the data and is based on the first-order Padé approximation (Laan *et al.* 2014)

$$\left(\beta_{max}^2 - \beta_{V_i\to 0}^2\right)^{1/2} Re^{-1/5} = We^{1/2}/(A + We^{1/2}). \tag{3.6}$$

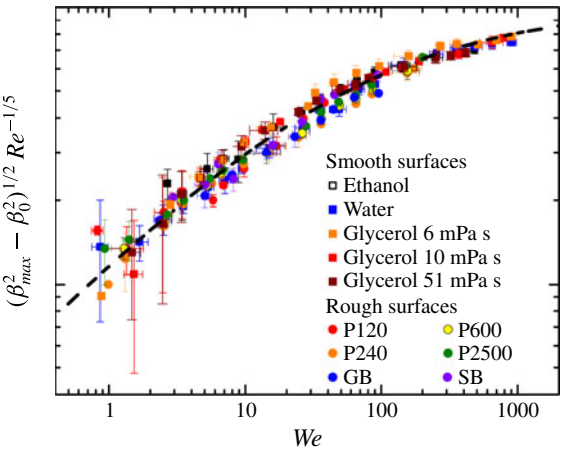

FIGURE 6. The rescaled maximum spreading ratio as a function of the Weber number in a log–log plot for all liquids and smooth and rough surfaces. The dotted line is the first-order Padé approximation (3.6).

Figure 6 shows the rescaled measured data $(\beta_{max}^2 - \beta_{V_i\to 0}^2)^{1/2}$ versus the Weber number. We observe that all rescaled data, for all liquids and all substrates (roughness, nature), collapse onto a single curve. In addition, using this approach it is shown that, for low impact velocities the maximum spreading ratio approaches $\beta_{V_i\to 0}$ and for high impact velocities, we find once more the $Re^{1/5}$ scaling. Moreover, the transition from low impact velocity towards high impact velocity is a function of $We^{1/2}$. The curve as predicted by (3.6) ($A = 7.6$) describes the data very well. The larger error bars at low velocity are due to the logarithmic scaling.

This result shows that we universally rescale the maximum spreading ratio for different liquids and substrates into a single description, when the dynamic wettability is taken into account accurately.

4. Conclusion

We show that a universal scaling can be used to describe the maximum spreading of liquid droplets impacting on smooth and rough surfaces from low to high impact velocity. At low impact velocity the droplet spreading follows a scaling with $We^{1/2}$ after correcting for dynamic wetting behaviour. The dynamic wetting is described by the maximum spreading at zero velocity, which can be related to a corresponding contact angle using the spherical cap model. Although the spherical cap model shows some limitation in describing the droplet shape at maximum spreading, we demonstrate that the contact angle describing the wetting behaviour at low impact velocity correlates with the dynamic contact angle at maximum spreading, as determined in our measurements. The influence of the liquid as well as the nature and roughness of the surface are properly taken into account by the rescaling. We demonstrate that all data for different liquids and substrates collapse onto a single curve by taking into account the dynamic wetting behaviour at low impact velocity. The results of this study are important for a wide range of applications for which the control of droplet deposition is of prominent importance.

Acknowledgements

The authors acknowledge the support of Swiss National Science Foundation grant no. 200021_135510. This research is supported by the Dutch Technology Foundation STW, which is part of the Netherlands Organization for Scientific Research (NWO) and which is partly funded by the Ministry of Economic Affairs, Agriculture and Innovation. Acknowledgements go to H. Schlatter for R_a measurements.

References

ABUKU, M., JANSSEN, H., POESEN, J. & ROELS, S. 2009 Impact, absorption and evaporation of raindrops on building facades. *Build. Environ.* **44** (1), 113–124.

BECHTEL, S. E., BOGY, D. B. & TALKE, F. E. 1993 Impact of a liquid drop against a flat surface. *IBM J. Res. Dev.* **25** (6), 963–971.

BERGERON, V., BONN, D., MARTIN, J. Y. & VOVELLE, L. 2000 Controlling droplet deposition with polymer additives. *Nature* **405** (6788), 772–775.

BERTHIER, E. & BEEBE, D. J. 2007 Flow rate analysis of a surface tension driven passive micropump. *Lab on a Chip* **7** (11), 1475–1478.

BIOLÈ, D. & BERTOLA, V. 2015 A goniometric mask to measure contact angles from digital images of liquid drops. *Colloids Surf.* A **467**, 149–156.

BLOCKEN, B. & CARMELIET, J. 2015 Impact, runoff and drying of wind-driven rain on a window glass surface: numerical modelling based on experimental validation. *Build. Environ.* **84**, 170–180.

CHANDRA, S. & AVEDISIAN, C. T. 1991 On the collision of a droplet with a solid surface. *Proc. R. Soc. Lond.* A **432**, 13–41.

CLANET, C., BÉGUIN, C., RICHARD, D. & QUÉRÉ, D. 2004 Maximal deformation of an impacting drop. *J. Fluid Mech.* **517**, 199–208.

COLLINGS, E. W., MARKWORTH, A. J., MCCOY, J. K. & SAUNDERS, J. H. 1990 Splat-quench solidification of freely falling liquid-metal drops by impact on a planar substrate. *J. Mater. Sci.* **25** (8), 3677–3682.

DERBY, B. 2010 Inkjet printing of functional and structural materials: fluid property requirements, feature stability, and resolution. *Annu. Rev. Mater. Res.* **40** (1), 395–414.

EGGERS, J., FONTELOS, M. A., JOSSERAND, C. & ZALESKI, S. 2010 Drop dynamics after impact on a solid wall: theory and simulations. *Phys. Fluids* **22** (6), 062101.

ERKAL, A., D'AYALA, D. & SEQUEIRA, L. 2012 Assessment of wind-driven rain impact, related surface erosion and surface strength reduction of historic building materials. *Build. Environ.* **57**, 336–348.

JOUNG, Y. S. & BUIE, C. R. 2015 Aerosol generation by raindrop impact on soil. *Nature Commun.* **6**, 6083.

LAAN, N., DE BRUIN, K. G., BARTOLO, D., JOSSERAND, C. & BONN, D. 2014 Maximum diameter of impacting liquid droplets. *Phys. Rev. Appl.* **2**, 044018.

LAAN, N., DE BRUIN, K. G., SLENTER, D., WILHELM, J., JERMY, M. & BONN, D. 2015 Bloodstain pattern analysis: implementation of a fluid dynamic model for position determination of victims. *Sci. Rep.* **5**, 11461.

MADEJSKI, J. 1976 Solidification of droplets on a cold surface. *Intl J. Heat Mass Transfer* **19** (9), 1009–1013.

MCDONALD, A., LAMONTAGNE, M., MOREAU, C. & CHANDRA, S. 2006 Impact of plasma-sprayed metal particles on hot and cold glass surfaces. *Thin Solid Films* **514** (1–2), 212–222.

PASANDIDEH-FARD, M., QIAO, Y. M., CHANDRA, S. & MOSTAGHIMI, J. 1996 Capillary effects during droplet impact on a solid surface. *Phys. Fluids* **8** (3), 650.

RIOBOO, R., TROPEA, C. & MARENGO, M. 2001 Outcomes from a drop impact on solid surfaces. *Atomiz. Sprays* **11**, 155–165.

ROISMAN, I. V., RIOBOO, R. & TROPEA, C. 2002 Normal impact of a liquid drop on a dry surface: model for spreading and receding. *Proc. R. Soc. Lond.* A **458** (2022), 1411–1430.

WIRTH, W., STORP, S. & JACOBSEN, W. 1991 Mechanisms controlling leaf retention of agricultural spray solutions. *Pesticide Sci.* **33** (4), 411–420.

YARIN, A. L. 2006 Drop impact dynamics: splashing, spreading, receding, bouncing. . . . *Annu. Rev. Fluid Mech.* **38**, 159–192.

ZHAO, R., ZHANG, Q., TJUGITO, H. & CHENG, X. 2015 Granular impact cratering by liquid drops: understanding raindrop imprints through an analogy to asteroid strikes. *Proc. Natl Acad. Sci. USA* **112** (2), 342–347.